EFFECT OF DISTORTION ON THE STRUCTURAL BEHAVIOUR OF THIN-WALLED STEEL REGULAR POLYGONAL TUBES

RODRIGO GONÇALVES[1], DINAR CAMOTIM[2]

Abstract. This paper addresses the effect of cross-section distortion on the structural behaviour of thin-walled tubes with single-cell regular convex polygonal cross-sections (RCPS) and provides an in-depth view on the underlying mechanical aspects. In particular, the first-order, buckling (bifurcation) under uniform compression and undamped free vibration behaviours are characterised using the modal decomposition features and computational efficiency of a GBT (Generalised Beam Theory) specialization for RCPS recently developed by the authors [1]. Several analytical and illustrative numerical results are presented and discussed within the paper.

Key words: thin-walled members, regular polygonal cross-sections, cross-section distortion, Generalised Beam Theory (GBT), buckling behaviour, vibration behaviour.

1. INTRODUCTION

It is a well-known fact that cross-section distortion, which comprises both in-plane and out-of-plane (warping) displacements, can influence significantly the structural behaviour of open section thin-walled members. This phenomenon has been investigated rather intensively in the recent past and it may be argued that it is currently quite well understood, particularly for cold-formed steel lipped channel, zed, hat or "rack" section members. Much less known are the effects of distortion in thin-walled tubes with single-cell regular (equiangular and equilateral) convex polygonal cross-sections (RCPS), which are widely employed in slender structures such as lighting posts and telecommunication towers. The first papers on this subject were published only in the last year [1–3], where it was shown that, besides the well-known global and local (plate-type) deformation modes, the distortional modes also play a key role in the structural response of RCPS tubes, even in the case of geometrically linear problems.

This paper addresses specifically the influence of cross-section distortion on the structural behaviour of RCPS tubes and aims at providing a general and broad

[1] UNIC, Faculdade de Ciências e Tecnologia, Department of Civil Engineering, NOVA University Lisbon, 2829-516 Caparica, Portugal

[2] ICIST, Instituto Superior Técnico, Department of Civil Engineering, Architecture and Georesources, University of Lisbon, Av. Rovisco Pais, 1049-001 Lisbon, Portugal

perspective on the subject. The fundamental findings of the previous work are summarised and new results are reported, which further help characterising the distortional modes and also their relevance for the adequate assessment of the RCPS tube first-order, buckling and vibration behaviours. The Generalised Beam Theory (GBT) specialisation for RCPS proposed in [1] is employed, leading to the identification of a well-defined set of fully uncoupled cross-section distortional deformation modes. This approach also makes it possible to derive analytical or semi-analytical formulae that provide in-depth information concerning the structural behaviour of RCPS tubes.

The outline of the paper is as follows. Section 2 presents a brief overview of the GBT specialisation for RCPS and explores the features of the resulting orthogonal distortional deformation modes. Each of the subsequent sections focuses on a specific type of analysis, namely first-order (Section 3), linearised buckling under uniform compression (Section 4) and undamped free vibration (Section 5). Although GBT-based finite elements may be always employed to obtain numerical results, namely for arbitrary loading and/or boundary conditions, attention is devoted to analytical or semi-analytical solutions, which generally enable a better grasp of the underlying mechanical aspects. The paper closes in Section 6, with some concluding remarks.

The cross-section geometric parameters employed in this paper are indicated in Fig. 1(a), together with the non-dimensional parameters and relations

$$\beta_1 = \frac{L}{r}, \qquad \beta_2 = \frac{r}{t}, \qquad \frac{b}{t} = 2\beta_2 \sin\frac{\pi}{n}, \tag{1}$$

where L is the tube length. The material parameters are E (Young's modulus), G (shear modulus), ν (Poisson's ratio) and ρ (volumetric mass density).

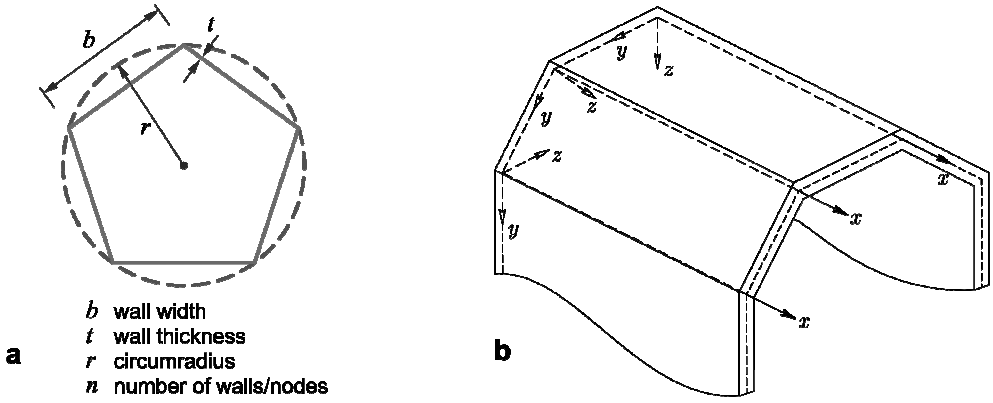

Fig. 1 – a) Geometry and notation for RCPS;
b) wall mid-surface local coordinate systems.

2. GBT FOR REGULAR CONVEX POLYGONAL TUBES

Following the notation of [4] and using the wall mid-surface local coordinate systems shown in Fig. 1(b), the GBT displacement field for each wall is given by

$$\begin{bmatrix} U_x \\ U_y \\ U_z \end{bmatrix} = \begin{bmatrix} u(x,y) - z w_{,x}(x,y) \\ v(x,y) - z w_{,y}(x,y) \\ w(x,y) \end{bmatrix}, \qquad \begin{aligned} u(x,y) &= \sum_{k=1}^{D} \overline{u}_k(y)\phi_{k,x}(x), \\ v(x,y) &= \sum_{k=1}^{D} \overline{v}_k(y)\phi_k(x), \\ w(x,y) &= \sum_{k=1}^{D} \overline{w}_k(y)\phi_k(x), \end{aligned} \tag{2}$$

where: (i) the comma indicates a partial differentiation, (ii) u, v, w are the mid-surface displacement components along x, y, z, respectively, (iii) the "bars" identify the associated deformation mode components, (iv) D is the number of deformation modes and (v) ϕ_k are their amplitude functions along the length of the beam (the problem unknowns).

The cross-section deformation modes (i.e., functions $\overline{u}_k, \overline{v}_k, \overline{w}_k$) are obtained from the "GBT cross-section analysis", which consists essentially of defining an initial set of modes and, then, sequentially solving a set of eigenvalue problems that partially uncouple the differential equilibrium equation system. A hierarchic set of deformation modes is then retrieved, which includes the classic prismatic beam theory modes (axial extension, bending about principal axes and torsion about the shear centre) and also the so-called "local", "distortional", "shear" and "transverse extension" deformation modes. This work focuses on the "natural Vlasov warping modes", obtained under the assumption of null membrane (i) shear strains (Vlasov's hypothesis) and (ii) transverse extensions (i.e., the walls are deemed inextensible in the cross-section plane). Then, in each wall, the $\overline{v}_k$ functions are constant and the $\overline{u}_k$ (warping) functions are linear. An initial base for these modes is obtained by (i) imposing unit warping displacements at each wall junction (cross-section "natural node"), (ii) calculating the $\overline{v}_k$ functions that ensure null membrane shear strains and, finally, (iii) obtaining the $\overline{w}_k$ functions by analysing the cross-section as a plane frame subjected to imposed $\overline{v}_k$ displacements.

RCPS constitute a rather distinctive "special case" amongst cross-section geometries. Indeed, these cross-sections exhibit rotational symmetry of order equal to the number of walls and nodes (n), a feature that is at the root of some remarkable peculiar features. In particular, the deformation mode configurations

obtained by imposing a single unit nodal warping displacement constitute rotations of each other. This implies that the resulting GBT modal matrices, given in Annex B, are symmetric and circulant and, therefore, may be diagonalised by means of $\mathbf{Q}^{\mathrm{t}}\mathbf{A}\mathbf{Q}$, where $\mathbf{A}$ is a GBT modal matrix and $\mathbf{Q}$ is a matrix whose columns are given by vectors $\boldsymbol{a}^{(l)}$ and $\boldsymbol{b}^{(l)}$, whose components read [1]

$$\begin{aligned} a_j^{(l)} &= \cos\left(\frac{2\pi jl}{n}\right), \qquad l = 0,\ldots,\left[\frac{n}{2}\right], \\ b_j^{(l)} &= \sin\left(\frac{2\pi jl}{n}\right), \qquad l = 1,\ldots,\left[\frac{n-1}{2}\right], \end{aligned} \tag{3}$$

where $[k]$ designates the largest integer not exceeding k. Each vector corresponds to a specific orthogonal warping function, where component j contains the warping at node j. In particular:

(i) For $l = 0$, one has $a_j^{(0)} = 1$, which corresponds to constant warping at the cross-section, i.e., to the classic axial extension mode.

(ii) For each $l = 1,\ldots, (n–1)/2$, two deformation modes are obtained, associated with warping functions having l full cycles around the cross-section. Bending about orthogonal axes corresponds to $l = 1$, i.e., warping functions with one full cycle and neutral axes rotated by $\pi/2$. The subsequent deformation mode pairs are termed "distortional", since cross-section in-plane displacements of the natural nodes are involved (besides warping). As discussed in [1], the two diagonal components of $\mathbf{Q}^{\mathrm{t}}\mathbf{A}\mathbf{Q}$ corresponding to each l are identical. Furthermore, it can be shown that a combination of the mode pair of the form

$$a_j^{(l)} \cos\theta + b_j^{(l)} \sin\theta, \tag{4}$$

where θ is the rotation angle in the two-dimensional mode space, does not change the matrix diagonal component. The fact that the stiffness properties of the deformation mode pairs (the GBT matrix components) are invariant with respect to θ constitutes an important generalisation of the bending behaviour of RCPS tubes, where all central axes are principal bending axes – bending may now be viewed as just the particular case of $l = 1$. Finally note that, in order to obtain bending deformation modes associated with unit curvatures, the corresponding warping functions must be multiplied by r (this was not done in the present paper).

(iii) For $l = n/2$, which only applies to cross-sections with even n, a single distortional mode is obtained, which exhibits alternating positive and negative warping displacements at consecutive nodes.

Since the orthogonal RCPS warping functions are already known, it is a quite straightforward task to calculate the complete deformation mode shapes and the corresponding GBT matrix diagonal components – Annex A provides a set of expressions that can be employed for this purpose. In [1], some analytical formulae are given and all matrix components are shown in a graphical format, normalised with respect to the values for circular tubes.

For illustrative purposes, Table 1 provides the distortional mode matrix diagonal components, in a non-dimensional form, for n = 4-8, β_2=100 and ν = 0.3 (the parameters α and β appearing in the table are discussed in the next section). Furthermore, Fig. 2 shows the shapes of the natural Vlasov warping modes and the associated warping functions, as well as their sinusoidal counterparts, for n = 6. The analytical expressions providing the GBT matrix components are also shown in the figure – they were calculated using the expressions given in Annex B. As previously explained, this cross-section has 6 warping modes: axial extension (l = 0), the bending mode pair (l = 1), one distortional mode pair (l = 2) and a single distortional mode (l = 3).

Fig. 3(a) makes it possible to visualise the shapes of the distortional deformation modes for cross-sections with n = 4–8. Note that, as already mentioned, the distortional modes appear in pairs, with the exception of the $l = n/2$ mode for even n. Finally, Fig. 3b shows the effect of the rotation θ on the deformation mode shape, for the particular case of the l = 3 distortional pair of a cross-section with n = 20. The deformation modes obtained by means of Eqs. (3) correspond to $\theta = 0^o$ and $\theta = 90^o$.

Table 1
Distortional mode matrix diagonal components
and exponential solution parameters

n	l	C/Er^2 ($\times 10^{-3}$)	Br^2/E ($\times 10^{-6}$)	D/E ($\times 10^{-6}$)	αr ($\times 10^{-3}$)	βr ($\times 10^{-3}$)
4	2	18.86	12.43	4.97	113.6	113.0
5	2	11.67	18.59	7.57	141.8	140.7
6	2	15.00	26.37	12.09	145.5	144.1
	3	20.00	316.48	63.30	252.4	249.2
7	2	18.00	30.78	15.02	144.5	143.1
	3	11.13	390.85	72.40	308.7	303.4
8	2	20.41	33.47	16.90	143.0	141.6
	3	13.20	603.60	118.95	330.4	323.5
	4	20.42	3121.6	365.71	447.2	437.0

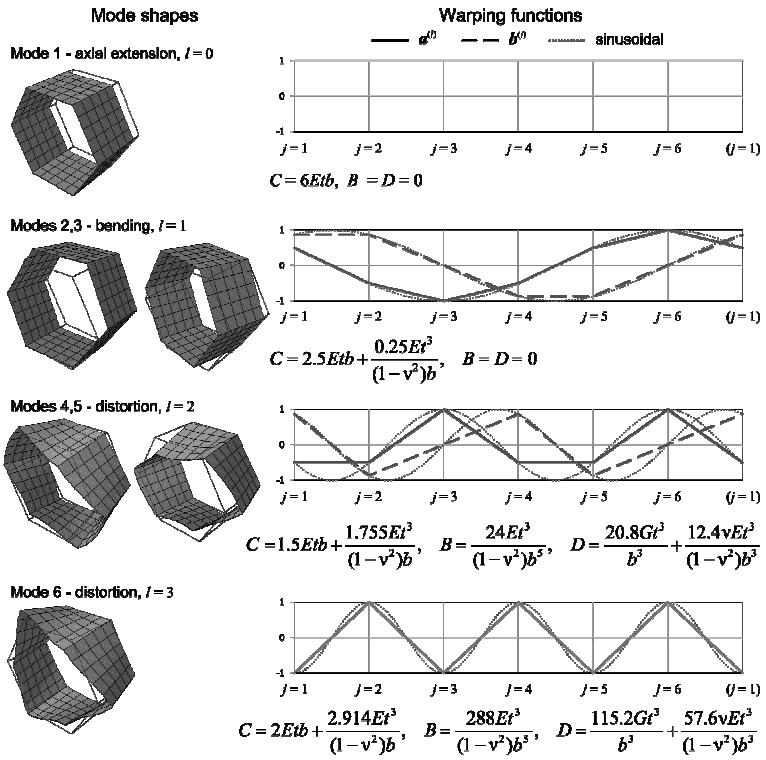

Fig. 2 – Hexagonal cross-section: shapes of the natural Vlasov warping modes and associated matrix components (the mode shapes are depicted assuming a linear amplitude function $\phi_k(x) = x$).

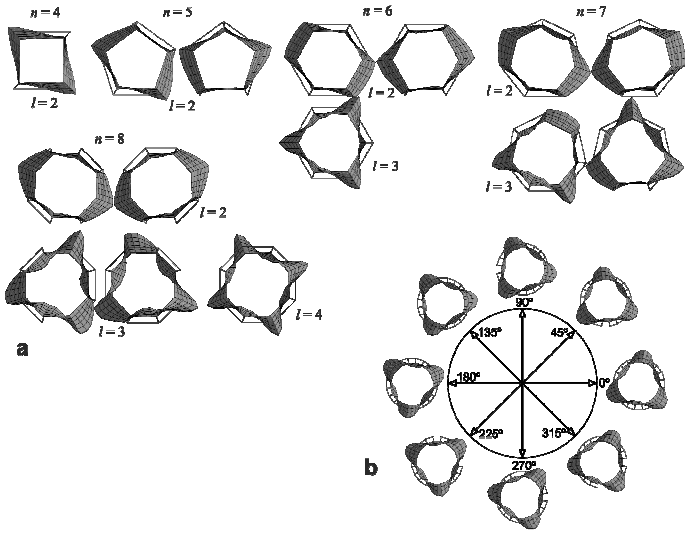

Fig. 3 – a) Distortional deformation modes for n = 4–8; b) distortional deformation mode configurations for n = 20 and l = 3, as a function of the rotation θ.

3. FIRST-ORDER BEHAVIOUR

This section addresses the influence of the distortional modes on the first-order (linear) behaviour of RCPS tubes. First, consider the homogeneous form of the GBT equilibrium differential equation system for RCPS, which is uncoupled and reads, for mode k,

$$C_{kk}\,\phi_{k,xxxx} - D_{kk}\,\phi_{k,xx} + B_{kk}\,\phi_k = 0, \tag{5}$$

where D_{kk} and B_{kk} are null for the axial extension and bending deformation modes. In long tubes, the general solution for the distortional modes is given by [5]

$$\begin{aligned} &\phi_k = e^{-\alpha x}\left(A_1 \sin\beta x + A_2 \cos\beta x\right), \\ &\alpha = \sqrt{\sqrt{\frac{B_{kk}}{4C_{kk}}} + \frac{D_{kk}}{4C_{kk}}}, \qquad \beta = \sqrt{\sqrt{\frac{B_{kk}}{4C_{kk}}} - \frac{D_{kk}}{4C_{kk}}}, \end{aligned} \tag{6}$$

where α is the exponential decay and β (herein assumed to be real) is the frequency of the sinusoid. The factors π/α and π/β provide a measure of the influence length of the deformation mode – note that, at $x = \pi/\alpha$, the exponential term is 4.32% and π/β corresponds to the half-wavelength. For the cross-sections indicated in Table 1, the influence length varies between about 30r and 7r, decreasing as l increases – i.e., the higher order deformation modes have a smaller influence length.

If at $x = 0$ (i) a diaphragm, restraining only the displacements along z, is introduced and (ii) a distortional-like stress distribution is applied, i.e.,

$$\sigma_{xx}(y) = \sum_{k=4}^{D} \lambda_k\, \overline{u}_k(y), \tag{7}$$

where λ_k is the stress amplitude of mode k (with $k \geq 4$, i.e., $l \geq 2$), one obtains, for each deformation mode, the constants $A_1 = -\lambda_k/2E\alpha\beta$ and $A_2 = 0$. For illustrative purposes, Fig. 4(a) plots the function $e^{-\alpha x}\sin\beta x$ for the distortional modes listed in Table 1, with respect to the normalised coordinate x/r – it is clearly shown that the influence length decreases with l (as already concluded) and also with n.

Consider now simply supported beams of length L and acted by sinusoidal lateral loads. In this case, the analytical solution is given by [1]

$$\phi_k = \overline{\phi}_k \sin\frac{\pi x}{L}, \quad \overline{\phi}_k = \frac{\overline{q}_k}{\frac{\pi^4}{L^4}C_{kk} + \frac{\pi^2}{L^2}D_{kk} + B_{kk}}, \quad \overline{q}_k = \overline{q}_y\overline{v}_k + \overline{q}_z\overline{w}_k, \tag{8}$$

where $\overline{q}_y, \overline{q}_z$ are the components of the distributed load along the local axes and $\overline{v}_k, \overline{w}_k$ are the modal displacement components at the cross-section point of load application.

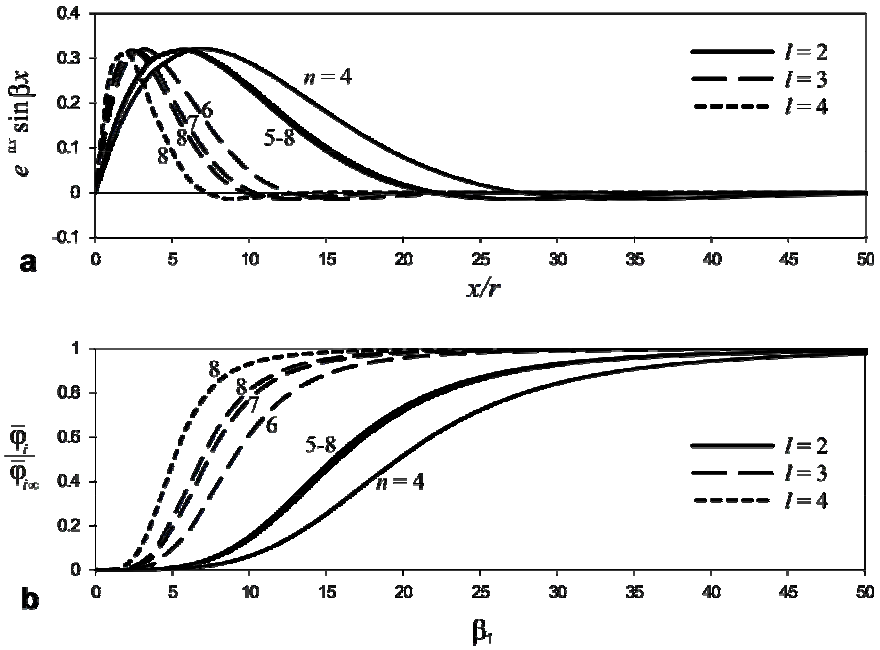

Fig. 4 – a) Exponential and b) sinusoidal solutions for the distortional modes indicated in Table 1 ($\beta_2 = 100$, $\nu = 0.3$).

This solution shows that, as L increases, the amplitude $\overline{\phi}_k$ increases and tends asymptotically to $\overline{q}_k / B_{kk}$. For the bending modes, one has B_{kk}= 0 and, therefore, the amplitude grows unboundedly with L.

The amplitude $\overline{\phi}_k$ may be written in a non-dimensional format, using the solution corresponding to an infinite beam span, which leads to

$$\frac{\overline{\phi}_k}{\overline{\phi}_{k\infty}} = \frac{1}{\frac{\pi^4}{\beta_1^4}\frac{C_{kk}}{B_{kk}r^4} + \frac{\pi^2}{\beta_1^2 B_{kk} r^2} D_{kk} + 1}. \tag{9}$$

Figure 4(b) plots the results obtained with the above expression, for the values shown in Table 1. Note that the solution for $L = \infty$ is approached more rapidly as n and l increase.

It is worth mentioning that a set of numerical examples involving distortional, torsional, bending and local deformation modes has been presented and discussed in [1]. In all of those examples, the GBT-based solutions were compared with the results provided by shell finite element models and an excellent agreement was invariably found.

4. BUCKLING BEHAVIOUR

This section presents the fundamental aspects of the distortional buckling (bifurcation) behaviour of RCPS tubes subjected to uniform compression. A more general discussion of the buckling behaviour of RCPS, including multi-mode interactions and the effects of bending or torsion, can be found in [2, 3].

For the classic benchmark problem of simply supported members under uniform compression, sinusoidal amplitude functions correspond to the exact solution and, therefore, one has, for each individual deformation mode k, (negative means compression)

$$(\sigma_b)_k = \frac{-1}{X_{kk}}\left(\frac{a^2\pi^2}{\beta_1^2}\frac{C_{kk}}{r^2} + D_{kk} + \frac{\beta_1^2}{a^2\pi^2}r^2 B_{kk}\right),$$
$$(\sigma_{cr})_k = -\frac{D_{kk} + 2\sqrt{C_{kk}B_{kk}}}{X_{kk}}, \qquad \left(\frac{\beta_1}{a}\right)_{cr} = \sqrt[4]{\frac{\pi^4 C_{kk}}{r^4 B_{kk}}}, \tag{10}$$

where: (i) σ_b is the bifurcation stress, (ii) σ_{cr} is the critical stress (the lowest σ_b), (iii) a is the buckling mode longitudinal half-wave number, (iv) $(\beta_1/a)_{cr}$ is the buckling mode normalised half-wavelength corresponding to σ_{cr} and (v) X_{kk} are the components of the GBT geometric modal matrix for uniform compression (see Annex B).

It can be shown that the minimum distortional critical buckling stress always corresponds to $l = 2$, i.e., to the first distortional deformation mode pair (or to the single distortional mode if $n = 4$). Moreover, the critical stresses associated with each l decrease as n increases and approach asymptotically the values corresponding to circular tubes – for instance, for $l = 2$ and $\beta_2 = 75$, the difference between the critical buckling stresses concerning columns exhibiting RCPS and circular hollow sections is below 4% for $n \geq 9$.

For the cross-sections listed in Table 1 ($\beta_2 = 100$, $\nu = 0.3$), the $(\beta_1/a)_{cr}$ values vary between 19.6 ($n = 4$ and $l = 2$) and 5 ($n = 8$ and $l = 4$) and, essentially, decrease when l and n increase. Note that these half wave-lengths are significantly higher than those associated with local buckling, which are of the order of the wall width b, i.e., $(\beta_1/a)_{cr}$ equal to (i) 1.4 for $n = 4$, (ii) 1.0 for $n = 6$ and (iii) 0.62 for $n = 8$.

The graph in Fig. 5(a) shows the parameter range values for which the critical buckling stress is either distortional or local [2]. These values were determined for $\nu = 0.3$ and assuming that no mode interaction occurs. It is concluded that distortional buckling is critical for the lower β_2 values but, as n increases, the critical buckling mode transition occurs for increasingly higher β_2 values.

As show in [2], the true distortional critical modes involve participations of local and shear deformation modes. The graph in Fig. 5(b) shows the variation of the distortional critical buckling stresses with n, determined by means of GBT analyses that include the following deformation mode sets: (i) Vlasov (distortional), (ii) Vlasov + shear and (iii) local + Vlasov + shear. It is observed that the shear modes play a

significant role, particularly for low β_2 values. The local modes are also relevant, but only for low n.

Finally, Fig. 5(c) presents an illustrative numerical example: it plots the variation of the buckling stresses with β_1/a, for the particular case defined by n = 10, r = 100 mm, t = 4 mm (β_2 = 25) and ν=0.3, which corresponds to almost coincident local and distortional

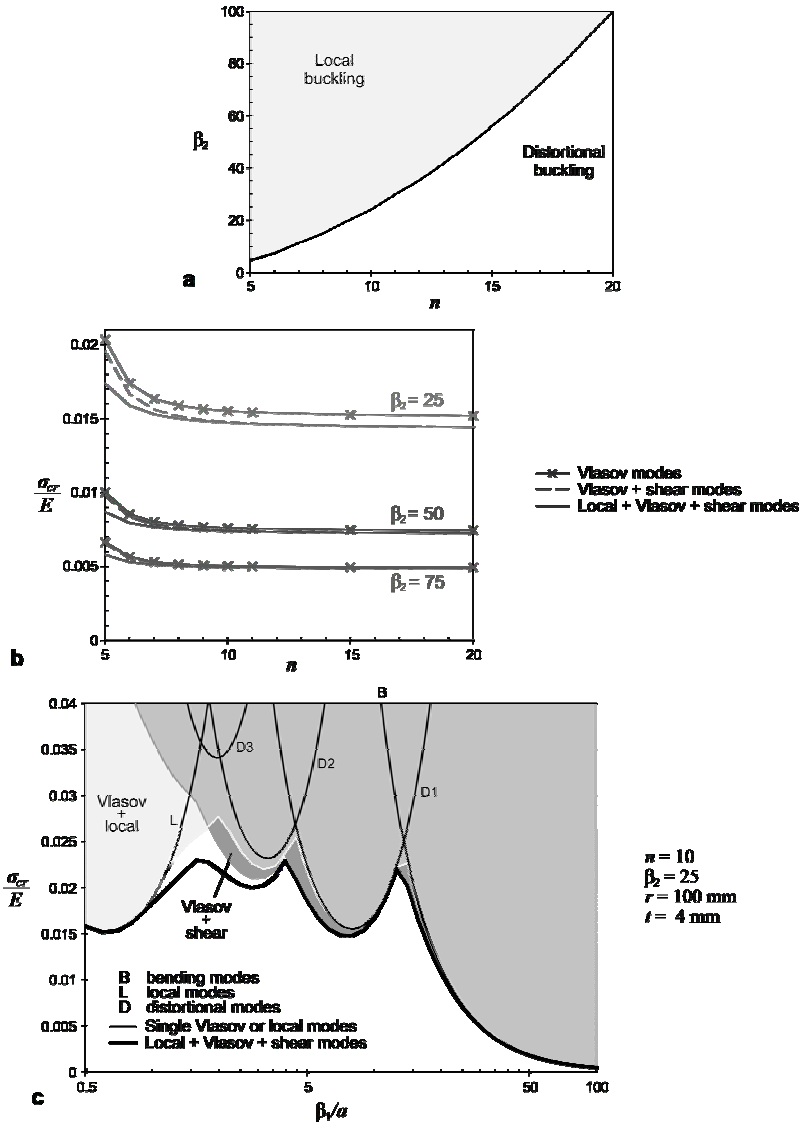

Fig. 5 – Buckling of simply supported RCPS tubes under uniform compression (ν = 0.3):
a) parameter ranges corresponding to critical "local and distortional" buckling;
b) influence of the local and shear modes on distortional buckling; c) illustrative example.

critical buckling stresses. This figure includes "single mode curves" and also curves obtained from analyses with various deformation mode sets, making it possible to conclude that the buckling mode nature changes with β_1/a in the following manner:

(i) For $\beta_1/a < 1.6$, local buckling governs (curve "L" in Fig. 5(c)). However, the distortional and shear deformation modes participate in the ascending branch of the curve, near the buckling mode transition zone.

(ii) For $1.6 < \beta_1/a < 4.0$, the second distortional mode pair ($l = 3$ – curve "D2") is critical, with significant participations from both the shear and local deformation modes.

(iii) For $4.0 < \beta_1/a < 13$, the first distortional mode pair ($l = 2$ – curve "D1") governs and, as already concluded from Fig. 5(b), the shear modes have a significant influence, particularly in the descending branch.

(iv) For $\beta_1/a > 13$, the buckling mode involves global bending (curve "B") and the shear modes have a small participation up to $\beta_1/a = 20$.

5. VIBRATION BEHAVIOUR

Although GBT is mostly employed for buckling analyses, formulations have also been developed to analyse the vibration behaviour of thin-walled members (see, e.g., [6–8]). In this section, GBT analyses are used to investigate the undamped free vibration behaviour of RCPS tubes. As in the previous section, only simply supported members are dealt with, which means that sinusoidal amplitude functions constitute exact solutions and, therefore, the "single mode solution" is given by

$$\omega_k^2 = \frac{\dfrac{a^2\pi^2}{\beta_1^2}\dfrac{C_{kk}}{r^2} + D_{kk} + \dfrac{\beta_1^2}{a^2\pi^2} r^2 B_{kk}}{Q_{kk} + \dfrac{\beta_1^2}{a^2\pi^2} r^2 R_{kk}}, \qquad (\omega_k)_{\min} = \sqrt{B_{kk}/R_{kk}}, \tag{11}$$

where (i) ω is the natural angular frequency, (ii) a is the vibration mode longitudinal half-wave number and (iii) the expressions for the mass matrices **Q** and **R** are given in Annex B. These formulae show that, since B_{kk} and D_{kk} are non-null for each distortional mode, the corresponding frequency always decreases with β_1/a and the minimum is attained at $\beta_1/a = \infty$. Moreover, as in the case of buckling under uniform compression, it can be shown that the minimum distortional frequency always corresponds to $l = 2$ and, as n increases, it approaches the solution for circular tubes.

Figure 6 shows the variation of the fundamental frequency with β_1/a, for the particular cases of $n = 6$, $\beta_2 = 25$, 100 and $\nu = 0.3$. The frequencies are normalised with respect to the fundamental frequency of a simply supported rectangular plate of infinite length, width b and thickness t, which is given by

$$f_0 = \frac{\pi}{2b^2}\sqrt{\frac{D_f}{\rho t}}, \tag{12}$$

where $D_f = Et^3/12(1-\nu^2)$ is the plate bending stiffness and ρ is the volumetric mass density. The plots show "single mode solutions" and results obtained by means of analyses including all the deformation modes, namely the shear and local modes. The observation of these results prompts the following remarks:

(i) The fundamental vibration mode nature changes with β_1/a as follows: (i_1) local for low β_1/a (curves "L"), (i_2) first distortional mode pair ($l = 2$ – curves "D1") for intermediate β_1/a and (i_3) global bending for high β_1/a (curves "B").

(ii) With the exception of the transition zone between the local and distortional vibration modes, the individual mode solutions provide accurate solutions.

(iii) Although this is not shown in Fig. 6, in the local-distortional transition zone the vibration mode is affected by local-distortional interaction and also by the shear modes. The maximum influence of the shear modes is about 7% and occurs for $\beta_2 = 25$ and $\beta_1/a = 4$, which corresponds to the initial stage of the transition zone. For $\beta_2 = 100$, the influence of the shear modes drops to a maximum of only 1.7%.

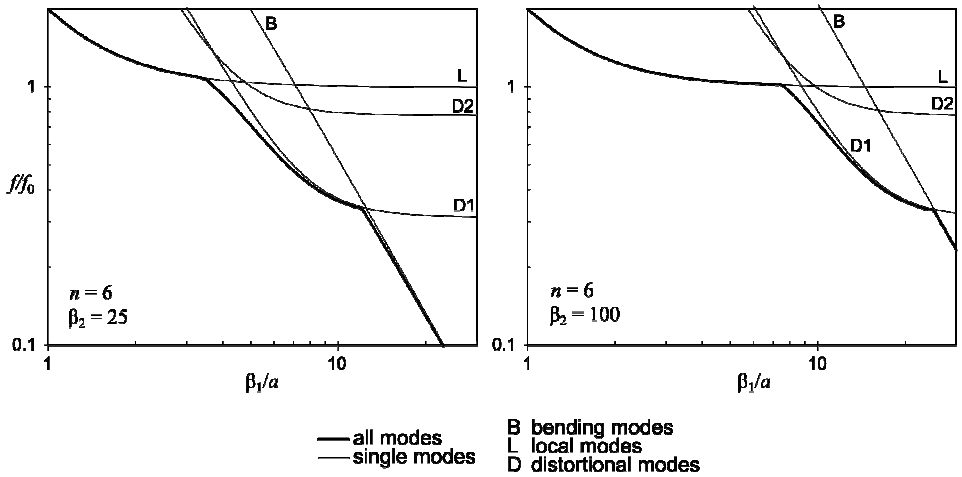

Fig. 6 – Normalised fundamental frequencies for simply supported RCPS tubes ($n = 6$, $\beta_2 = 25$, 100, $\nu = 0.3$)

6. CONCLUDING REMARKS

This paper addressed the effect of cross-section distortion on the: (i) first-order, (ii) buckling (bifurcation) under uniform compression and (iii) undamped free vibration behaviour of thin-walled RCPS tubes. In particular, attention is called to the following findings of the work carried out:

(i) Duplicate solutions are obtained for cross-sections with more than four walls, due to the cross-section rotational symmetry. This implies that the stiffness properties associated with the duplicate deformation modes are invariant upon a rotation in the two-dimensional mode space.

(ii) The GBT specialisation for RCPS makes it possible to identify a set of uncoupled and hierarchic distortional deformation modes. The exponential solutions show that the higher-order distortional modes decay more rapidly and, therefore, have a smaller influence length.

(iii) The distortional deformation modes play a significant role in the buckling and vibration behaviour of RCPS tubes. It was shown that, for some parameter ranges, the distortional modes correspond to the critical modes/fundamental frequencies.

(iv) It was also shown that local/distortional/shear interaction is relevant, particularly in mode transition zones.

ANNEX A: CROSS-SECTION ANALYSIS FOR RCPS

In a circulant matrix, all rows correspond to cyclic permutations of a single row vector, with an offset equal to the row index. The generating row vector is herein defined as the first row of the matrix. For instance, for a given 4×4 matrix **A**, one has

$$A = (A_{11}, A_{12}, A_{13}, A_{14}) \tag{A.1}$$

and, if the matrix is symmetric, one has $A_{12} = A_{14}$. Due to the rotational symmetry of RCPS, the GBT cross-section analysis involves several circulant matrices, which lead to rather simple expressions.

Fig. A1 shows, for the particular case of $n = 5$, (a) the node/wall numbering and local axes, and (b) the statically determinate system adopted to perform the usual GBT cross-section analysis and the convention for positive nodal moments. Let $(U_x)_{ij}$, V_{ij}, $\Delta\Theta_{ij}$, M_{ij} be $n \times n$ matrices, whose components contain, respectively, (i) the $\overline{u}$ nodal displacements, (ii) the wall $\overline{v}$ displacements, (iii) the converging wall relative rotations and (iv) the nodal moments. In these matrices, j identifies the

deformation mode and i concerns the node/wall number. As discussed in Section 2, the orthogonal warping deformation modes are already given by $\mathbf{U}_x = \mathbf{Q}$ and, from the null membrane shear strain assumption, the $\bar{v}$ displacements are obtained as

$$\mathbf{V} = \frac{1}{b}\widetilde{\mathbf{V}}\mathbf{Q}, \qquad \widetilde{V} = (1, -1, 0, ..., 0), \tag{A.2}$$

where the auxiliary matrix $\widetilde{\mathbf{V}}$ is circulant. The complete cross-section in-plane configuration is determined by imposing $\bar{v}$ displacements in the static system, using the flexibility/force method, which is convenient in this case (the degree of static indeterminacy is lower than the degree of kinematic indeterminacy). Simple geometric considerations make it possible to conclude that the imposed relative rotations in the pin-jointed frame are given by

$$\Delta\boldsymbol{\Theta} = \frac{1}{b\sin\psi}\Delta\widetilde{\boldsymbol{\Theta}}\mathbf{V}, \qquad \Delta\widetilde{\Theta} = (-2\cos\psi - 1, 1, 0, ..., 0, -1, 2\cos\psi + 1), \tag{A.3}$$

where $\psi = 2\pi/n$ is the angle between two adjacent walls.

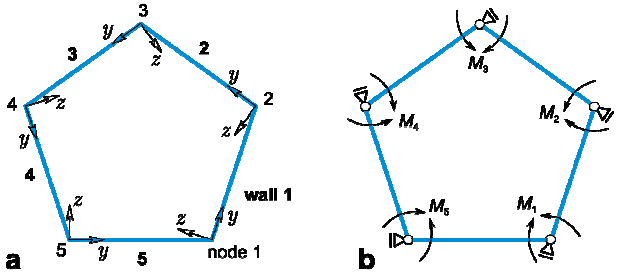

Fig. A1 – GBT cross-section analysis for n = 5: a) node/wall numbering and local axes; b) statically determinate pin-jointed frame and convention for positive nodal moments

The matrix equation to be solved is then

$$\frac{b}{6D_f}\widetilde{\mathbf{F}}\mathbf{M} = -\Delta\boldsymbol{\Theta}, \tag{A.4}$$

where the normalised flexibility matrix $\widetilde{\mathbf{F}}$ is symmetric and circulant, with

$$\widetilde{F} = (4, 1, 0, ..., 0, 1). \tag{A.5}$$

In order to solve the system (A.4), one may diagonalize the symmetric circulant matrix through $\mathbf{Q}^t\mathbf{F}\mathbf{Q}$=diag($\hat{F}_i$), where $\hat{F}_i$ is the i^{th} diagonal component (instead of directly inverting $\widetilde{\mathbf{F}}$). This leads to

$$\mathbf{M} = -\frac{6D_f}{b^3\sin\psi}\mathbf{Q}\,\mathrm{diag}\left(\frac{1}{\hat{F}_i}\right)\mathbf{Q}^t\,\Delta\widetilde{\boldsymbol{\Theta}}\widetilde{\mathbf{V}}\mathbf{Q}. \tag{A.6}$$

The $\overline{w}$ displacements associated with each deformation mode are obtained from the integration of the nodal moments of the corresponding column of **M**.

In [1], analytical formulae for matrix $\mathbf{C}^M$ are provided and all matrix components are shown in a graphical format. Using the former expressions, it is now possible to obtain the (diagonal) components of matrix **B** from the rather simple formula

$$B_{ii}^B = \frac{b}{3D_f}\sum_{j=1}^{n}\left(M_{ji}^2 + M_{(j+1)i}^2 + M_{ji}M_{(j+1)i}\right), \tag{A.7}$$

where $j+1=1$ if $j=n$.

ANNEX B: GBT MODAL MATRICES

Assuming null membrane shear strains and null membrane transverse extensions, the classic GBT modal stiffness matrices read

$$\begin{aligned}
&B_{ij} = B_{ij}^B = \int_S D_f\, \overline{w}_{i,yy}\overline{w}_{j,yy}\, \mathrm{d}y,\\
&C_{ij} = C_{ij}^M + C_{ij}^B = \int_S \left(Et\,\overline{u}_i\overline{u}_j + D_f\,\overline{w}_i\overline{w}_j\right)\mathrm{d}y,\\
&\mathbf{D} = \mathbf{D}_1 - \mathbf{D}_2 - \mathbf{D}_2^t,\\
&\left(D_1\right)_{ij} = \left(D_1\right)_{ij}^B = \int_S \frac{Gt^3}{3}\overline{w}_{i,y}\overline{w}_{j,y}\, \mathrm{d}y,\\
&\left(D_2\right)_{ij} = \left(D_2\right)_{ij}^B = \int_S \nu D_f\, \overline{w}_{i,yy}\overline{w}_j\, \mathrm{d}y,
\end{aligned} \tag{B.1}$$

where: (i) *M* and *B* designate membrane and bending terms, (ii) $i, j = 1, ..., D$, (iii) *S* is the cross-section mid-line, (iv) *t* is the wall thickness, (v) *E* and *G* are Young's and shear moduli and (vi) ν is Poisson's ratio. For buckling analyses of uniformly compressed members, the geometric matrix reads

$$X_{ij} = \int_S t\left(\overline{v}_i\overline{v}_j + \overline{w}_i\overline{w}_j\right)\mathrm{d}y. \tag{B.2}$$

Finally, for vibration analyses, the mass matrices **Q** and **R**, which involve translational and rotational terms, are given by

$$\begin{aligned}
&Q_{ij} = \int_S \rho\left(t\,\overline{u}_i\overline{u}_j + \frac{t^3}{12}\overline{w}_i\overline{w}_j\right)\mathrm{d}y,\\
&R_{ij} = \int_S \rho\left(t\left(\overline{v}_i\overline{v}_j + \overline{w}_i\overline{w}_j\right) + \frac{t^3}{3}\overline{w}_{i,y}\overline{w}_{j,y}\right)\mathrm{d}y,
\end{aligned} \tag{B.3}$$

where ρ is the volumetric mass density.

Received on: July 16, 2014

REFERENCES

1. GONÇALVES, R., CAMOTIM, D., *On the behaviour of thin-walled steel regular polygonal tubular members*, Thin-Walled Structures, **62**, pp. 191–205, 2013.
2. GONÇALVES, R., CAMOTIM, D., *Elastic buckling of uniformly compressed thin-walled regular polygonal tubes*, Thin-Walled Structures, **71**, pp. 35–45, 2013.
3. GONÇALVES, R., CAMOTIM, D., *Buckling behaviour of thin-walled regular polygonal tubes subjected to bending or torsion*, Thin-Walled Structures, **73**, pp. 185–97, 2013.
4. GONÇALVES, R., RITTO-CORRÊA, M., CAMOTIM, D., *A new approach to the calculation of cross-section deformation modes in the framework of Generalized Beam Theory*, Computational Mechanics, **46**, *5*, pp. 759–81, 2010.
5. SCHARDT, R., *Verallgemeinerte Technische Biegetheorie*, Springer-Verlag, Berlin, 1989.
6. SCHARDT, R., HEINZ, D., *Vibrations of thin-walled prismatic structures under simultaneous static load using Generalized Beam Theory*, in: *Structural Dynamics*, eds. W. Kratzig *et al*., Balkema, Rotterdam, 1991, pp. 921–927.
7. SILVESTRE, N., CAMOTIM, D., *GBT-based local and global vibration analysis of loaded composite open-section thin-walled members*, International Journal of Structural Stability and Dynamics, **6**, *1*, pp. 1–29, 2006.
8. BEBIANO, R., SILVESTRE, N., CAMOTIM, D., *Local and global vibration of thin-walled members subjected to compression and non-uniform bending*, Journal of Sound and Vibration, **315**, *3*, pp. 509–535, 2008.